ACS APPLIED MATERIALS & INTERFACES

Research Article

www.acsami.org

Synthesis of Eco-Friendly $CuInS_2$ Quantum Dot-Sensitized Solar Cells by a Combined Ex Situ/in Situ Growth Approach

Chia-Chan Chang,[†] Jem-Kun Chen,[‡] Chih-Ping Chen,[§] Cheng-Hsien Yang,[∥] and Jia-Yaw Chang*[,†]

[†]Department of Chemical Engineering, National Taiwan University of Science and Technology, 43, Section 4, Keelung Road, Taipei 10607, Taiwan, Republic of China

[‡]Department of Materials Science and Engineering, National Taiwan University of Science and Technology, 43, Section 4, Keelung Road, Taipei 10607, Taiwan, Republic of China

[§]Department of Materials Engineering, Ming Chi University of Technology, 84 Gungjuan Road, Taishan, New Taipei City 24301, Taiwan, Republic of China

[∥]ShiFeng Technology Co., Ltd., 31 Gongye 2nd Road, Annan, Tainan City 70955, Taiwan, Republic of China

Supporting Information

ABSTRACT: A cadmium-free $CuInS_2$ quantum dot (QD)-sensitized solar cell (QDSC) has been fabricated by taking advantage of the ex situ synthesis approach for fabricating highly crystalline QDs and the in situ successive ionic-layer adsorption and reaction (SILAR) approach for achieving high surface coverage of QDs. The ex situ synthesized $CuInS_2$ QDs can be rendered water soluble through a simple and rapid two-step method under the assistance of ultrasonication. This approach allows a stepwise ligand change from the insertion of a foreign ligand to ligand replacement, which preserves the long-term stability of colloidal solutions for more than 1 month. Furthermore, the resulting QDs can be utilized as sensitizers in QDSCs, and such a QDSC can deliver a power conversion efficiency (PCE) of 0.64%. Using the SILAR process, in situ $CuInS_2$ QDs could be preferentially grown epitaxially on the pre-existing seeds of ex situ synthesized $CuInS_2$ QDs. The results indicated that the $CuInS_2$ QDSC fabricated by the combined ex situ/in situ growth process exhibited a PCE of 1.84% (short-circuit current density = 7.72 mA cm^{-2}, open-circuit voltage = 570 mV, and fill factor = 41.8%), which is higher than the PCEs of $CuInS_2$ QDSCs fabricated by ex situ and in situ growth processes, respectively. The relative efficiencies of electrons injected by the combined ex situ/in situ growth approach were higher than those of ex situ synthesized $CuInS_2$ QDs deposited on TiO_2 films, as determined by emission-decay kinetic measurements. The incident photon-to-current conversion efficiency has been determined, and electrochemical impedance spectroscopy has been carried out to investigate the photovoltaic behavior and charge-transfer resistance of the QDSCs. The results suggest that the combined synergetic effects of in situ and ex situ $CuInS_2$ QD growth facilitate more electron injection from the QD sensitizers into TiO_2.

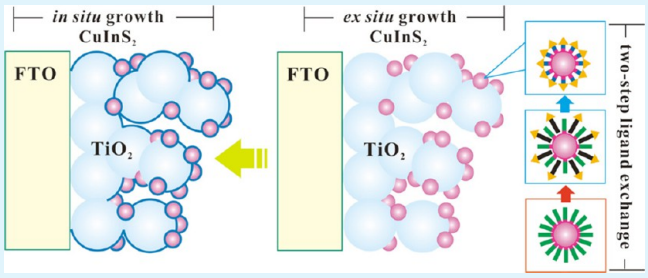

KEYWORDS: *quantum dots-sensitized solar cells, successive ionic-layer adsorption and reaction, $CuInS_2$, photoluminescence decay dynamics, photon-to-current conversion efficiency*

1. INTRODUCTION

Dye-sensitized solar cells have been considered promising alternatives to traditional silicon-based cells owing to their cost-effective manufacturing, high durability, and low environmental impact.[1,2] Furthermore, inorganic semiconductor quantum dots (QDs)[3−6] have been considered as a promising alternative to traditional sensitizers. Because the band gap of QDs can be controlled by simply changing their size, their optical properties can be tailored to maximize solar absorption. Moreover, QDs have been reported to produce highly efficient multiple charge carriers upon the absorption of a single photon owing to the impact ionization effect.[7,8] Thus, the power conversion efficiency (PCE) of QD-sensitized solar cells (QDSCs) is expected to exceed the Shockley−Queisser limit.[9] This is because photons with energies (E_{photon}) below the band gap energy (E_{gap}) are not absorbed, whereas those with energies above the band gap energy release the additional energy ($E_{photon} - E_{gap}$), mostly as heat.

Two distinct approaches have been reported for the synthesis of QDs attached to TiO_2 films: (1) deposition of ex situ[10] synthesized QDs on TiO_2 surfaces through direct adsorption or bifunctional-linker-assisted adsorption and (2) in situ synthesis of QDs on a semiconductor film by chemical-bath deposition (CBD) or the successive ionic-layer adsorption and reaction (SILAR) process. The first approach has the advantage of enabling a more accurate control of the size distribution and

Received: August 22, 2013
Accepted: October 6, 2013
Published: October 7, 2013

high crystallinity of the deposited QDs on TiO_2 electrodes. However, a low coverage of QDs on the electrode surface results in a low photovoltaic conversion efficiency. The second approach enables nucleation and in situ growth on TiO_2 electrodes, resulting in high surface coverage by QDs with better attachment to the electrode than can be achieved by the first approach. Moreover, the energy band of QDs can be tuned by varying their deposition cycle numbers. However, this approach gives limited control over the chemical composition, crystallinity, and spectral properties of QDs, and it results in a nonuniform size distribution.

A lot of effort based on the above approaches has been focused on the synthesis of II−VI and IV−VI QD sensitizers, such as cadmium or lead chalcogenide QDs, for use in QDSCs.[11−17] However, these semiconductor QDs are highly toxic and they easily disintegrate, leading to heavy-metal accumulation in subcellular regions when their surfaces are not appropriately passivated with either organic or inorganic shell protection.[18−21] The generation of environmentally "clean" energy requires not only the development of sustainable energy systems but also the elimination of hazardous precursors and the reduction of adverse environmental impact. Thus, the development of reliable eco-friendly protocols is of prime importance for QDSCs. Recently, environmentally friendly I−III−VI ternary semiconductor nanocrystals such as $CuInS_2$ have emerged as possible alternatives to the toxic metal-based QDs currently in use. These materials are of particular interest because they are direct band gap semiconductors with high extinction coefficients ($\sim 10^5$ cm^{-1}) in the visible-to-near-infrared region, can undergo facile electron/hole carrier conversion,[22] and do not contain any highly toxic elements. However, cadmium, a heavy metal,[23−28] is often used for improving the PCE of $CuInS_2$-based QDSCs. Therefore, the development of relatively high-performance, cadmium-free $CuInS_2$ QDSCs has become increasingly important and urgent for preventing the environmental problems caused by the currently used QDSCs.

In this study, we report a reliable and eco-friendly method based on a combination of ex situ and in situ QD growth approaches for synthesizing cadmium-free $CuInS_2$-based QDSCs with good photovoltaic performance. Ligand exchange with bifunctional ligands such as mercaptopropionic acid (MPA) has been extensively studied as a method for modifying the surface of ex situ synthesized QDs for phase transfer in QDSCs.[10,29−33] However, the ligand replacement ratio achieved by this method is typically low, resulting in colloidal instability.[34] This instability might impede the practical applications of QDSCs in the near future because good colloidal stability during long-term storage is necessary for realizing scalable and reproducible sensitizing ability using identical amounts of QDs on TiO_2 electrodes. Numerous synthetic methodologies for the production of I−III−VI QDs use 1-dodecanethiol as a capping agent because thiols provide the strongest chelating force for QDs.[35−42] During the early development stages of the ligand-exchange method, water-soluble II−VI QDs were generated by ligand exchange between the aliphatic surfactant of hydrophobic QDs and MPA. These preparative methods often used trioctylphosphine, tributylphosphine, or oleylamine and other long-chain amines as an aliphatic surfactant. Therefore, this approach might not be suitable for the production of I−III−VI QDs because 1-dodecanethiol and MPA possess identical sulfur-anchoring groups. In our method, ex situ synthesized $CuInS_2$ QDs allow easy stepwise change of the surface ligand via a two-step reaction: foreign-ligand insertion and alternative-ligand replacement. Oleic acid (OA), a naturally occurring monounsaturated omega-9 fatty acid with one cis double bond, was employed as the foreign ligand to loosen the original dense layer of pristine QDs for facilitating the sequential ligand exchange by MPA, thus enabling the QDs to tether on the TiO_2 surface. A thin layer of $CuInS_2$ was then uniformly coated on the surface of the ex situ synthesized $CuInS_2$ QDs by the in situ SILAR process, thus avoiding the use of any toxic chemicals during the synthesis. The relative efficiencies of electrons injected by the combined ex situ/in situ growth approach were higher than those of ex situ synthesized $CuInS_2$ QDs deposited on TiO_2 films, as determined by emission-decay kinetic measurements. $CuInS_2$-based QDSCs synthesized by the combined ex situ/in situ growth approach delivered the maximum PCE under the simulated illumination conditions of AM 1.5 and 100 mW cm^{-2}.

2. EXPERIMENTAL SECTION

2.1. Materials. Copper(II) nitrate hemipentahydrate ($Cu(NO_3)_2$, 98%), indium acetate ($In(Ac)_3$, 99.99%), and 3-mercaptopropionic acid (MPA, 99%) were purchased from Alfa-Aesar (Ward Hill, USA). Copper(I) iodide (CuI, 99.999%), indium(III) nitrate hydrate ($In(NO_3)_3$, 99.9%), oleic acid (OA, 65.0−88.0%), and sulfur powder (S, 99.98%) were purchased from Sigma-Aldrich (Milwaukee, USA). 1-Dodecanethiol (98%), potassium chloride (99+%), and sodium sulfide nonhydrate (Na_2S, 98+%) were purchased from Acros Organics (New Jersey, USA). Zinc acetate dehydrate ($Zn(Ac)_2$, 99.8%) was obtained from J. T. Baker (Phillipsburg, USA). All chemicals were used directly without further purification.

2.2. Preparation of $CuInS_2$ QDs. CuI (0.2 mmol) and $In(Ac)_3$ (0.8 mmol) were mixed with 10 mL of 1-dodecanethiol in a 50 mL three-necked flask with an attached Schlenk line. The mixture was stirred vigorously and degassed under vacuum, which was repeated for three cycles. Under Argon flow, the resulting solution was subsequently heated at 200 °C for 60 min. After the reaction was complete, the reaction mixture was cooled followed by the addition of 5 mL of $CHCl_3$ and centrifugation of the solution at 6000 rpm for 5 min. The supernatant was mixed with 5 mL of methanol and then precipitated by the addition of acetone followed by 20 min of centrifugation at 6000 rpm. The final product was redissolved in nonpolar solvents for characterization and surface modification.

2.3. Preparation of Water-Soluble $CuInS_2$ QDs via a Two-Step Method. $CuInS_2$ QDs (20 mg) were mixed with 120 μL of OA ligand under sonication for 1 h, subsequent to which 0.5 mL of hexane was introduced and another 10 min of sonication was performed. Then, 10 mL of aqueous solution was added into the resulting solution. For aqueous solution preparation, deionized water used was from a Millipore Alpha-Q purification system equipped with a 0.22 μm filter, and NaOH was used to adjust the pH value to 9. Ultrasonication (VCX 130 PB, 130 W, 20 kHz, Sonics and Materials Inc., Newton, CT) was performed by immersing an ultrasonic probe into the former mixture until the hexane and aqueous phases turned white and cloudy. The mixture was centrifuged at 6000 rpm for 15 min to speed the separation of the hexane and aqueous phases. Then, the aqueous solution was extracted and passed through a 0.22 μm filter to remove aggregated QDs. The concentration of water-soluble QDs was found to be 1 mg mL^{-1}. Subsequently, the resulting water-soluble QDs, with an absorbance value of 1.2 at the first excitonic absorption peak as recorded using a UV−vis spectrophotometer, were subjected to ligand exchange by mixing them with 0.5 M MPA under sonication for 1 h. The excess amount of ligand was isolated by centrifugation at 12 000 rpm for 10 min.

2.4. Preparation of Water-Soluble $CuInS_2$ QDs via a One-Pot Method. The preparation of water-soluble $CuInS_2$ QDs solution via one-pot method is described elsewhere.[43,44] MPA (0.2 mmol) was dissolved in 0.3 mL of deionized water together with 1.0 mL of

methanol, and the solution was then adjusted to pH 12 with the addition of 1.0 M NaOH. The resulting solution was then added to 5.0 mL of QD chloroform solution and stirred for 30 min for precipitation of the QDs. Subsequently, 10 mL of distilled water was added, and the mixture was vigorously stirred for 20 min. The water phase was separated from the organic phase, and acetone was then added for precipating the QDs. Finally, the pellet was redissolved in distilled water.

2.5. Device Fabrication. TiO_2 nanoparticles (Solaronix, Ti-Nanoxide T/SP) ~20 nm in size were screen-printed onto fluorine-doped tin oxide (FTO) glass substrate (TEC 7, Pilkington, USA.; sheet resistance: 8 Ω/□ and thickness: 2.2 mm). Subsequently, a dispersion of scattering TiO_2 particles (Solaronix, Ti-Nanoxide R/SP) were screen-printed on top of the transparent film; the film was then annealed at 500 °C for 30 min to form a double-layered mesoporous TiO_2 film. The as-prepared TiO_2 film was pretreated by soaking in 45 mL of acetonitrile containing 2 M MPA and 0.1 M H_2SO_4 for 24 h. For sensitization, the TiO_2 electrode was immersed in a sensitized solution of $CuInS_2$ QDs for another 24 h. The prepared $CuInS_2$-QDs-based TiO_2 electrodes were successively exposed to three different solutions: (1) 1.25×10^{-3} M $Cu(NO_3)_2$ in methanol for 30 s, (2) 1.35×10^{-1} M Na_2S in methanol/water (7:3, v/v) for 4 min, and (3) 10^{-1} M $In(NO_3)_3$ in methanol for 1 min. This SILAR process was repeated for two-to-six cycles until the desired TiO_2 photoanode was achieved. For the deposition of a ZnS passivation layer, the prepared TiO_2 photoanodes were immersed consecutively first in 0.03 M $Zn(Ac)_2$ in methanol and then in a solution of 0.03 M Na_2S in 50 mL of methanol/water (7:3, v/v) for 1 min each. Before each immersion, the electrodes were rinsed with pure methanol and dried under N_2 flow. This SILAR process was repeated for two cycles. After coating with the ZnS layer, the as-prepared TiO_2 photoanodes were then subjected to a sintering treatment in an oven at 250 °C for 3 min. Solar cells were fabricated by assembling the TiO_2 photoanodes and Cu_2S-deposited TCO glass as the counter electrode separated by a 60 μm thick Surlyn sheet (DuPont 1702). The Cu_2S-deposited counter electrode was prepared by spin coating of 200 μL (0.5 M) of $Cu(NO_3)_2$ in methanol for 30 s and 100 μL (0.5 M) of Na_2S in water for 30 s at a speed of 1000 rpm. This process was repeated for two cycles. The counter electrode was then subjected to calcination in an oven at 300 °C for 5 min. A polysulfide redox electrolyte consisting of 1.8 M Na_2S, 2.0 M sulfur, and 0.2 M potassium chloride in methanol/water (3:7, v/v) was introduced into the sealed cell (active area: 0.16 cm^2) by the capillary effect.

2.6. Sample Characterization. TEM imaging and energy-dispersive X-ray spectroscopy (EDS) of QDs were performed on a FEI Tecnai G2 F20 microscope (Philips, Holland) equipped with a field-emission gun working at an accelerating voltage of 200 kV. Field-emission scanning electron microscopy (SEM) was performed on a JEOL 6335F (JEOL USA Inc., USA) equipped with an EDS analysis. Powder X-ray diffraction (XRD) patterns were collected using a Rigaku 18 kW rotating anode source X-ray diffractometer with the Cu $K\alpha_1$ line (λ = 1.54 Å). Atomic force microscopy (AFM) observation was conducted using an SPM-9600 scanning probe microscope (Shimadzu Co.) at room temperature. The root mean square (rms) was used to evaluate the surface roughness of the QD films on the basis of a 5.0×5.0 μm^2 scan area. Cells used for AFM measurements did not employ TiO_2 light-scattering layers to avoid too large of a size difference between the TiO_2 nanoparticles and QDs. The rms represents the standard deviation of the height values within a given area and allows the surface roughness to be determined by statistical methods. It is given by

$$\mathrm{rms} = \sqrt{[\sum_{n=1}^{m} (z_n - z_{av})^2]/(m-1)} \quad (1)$$

where z_n is the current vertical distance value (z) and z_{av} represents the average of the z values within a given area of m data points. UV−vis absorption spectra were measured with a JASCO V-630 spectrometer. The measurements of photoluminescence (PL) spectra were carried out using a JASCO FP-6500 spectrofluorometer equipped with a 150 W xenon lamp. Time-resolved single-photon counting was performed with a (8 MHz) PicoQuant PDL 200-B pulsed diode laser at a wavelength of 450 nm, whereas the PL decay was monitored using a Jobin-Yvon H10 monochromator equipped with a PMA 185 photomultipier tube with a resolution of 30 ps (PicoQuant). The time-resolved decay curves were analyzed using the FluoFit software (PicoQuant, Germany) to extract the lifetime values. The instrument response function (IRF) of the TCSPC system has a width of 400 ps to provide 80 ps of time resolution with deconvolution. The quality of the curve fitting was evaluated by reduced chi-square (χ^2). The performance of a QDSC was assessed through measurement of a photocurrent density−photovoltage curve with an AM 1.5 G solar simulator (Oriel 6691 450-W xenon arc lamp, USA), calibrated with a NREL standard Si solar cell. The incident photon to current conversion efficiency (IPCE) plotted as a function of the excitation wavelength was measured with a PEC-S20 instrument (Peccell Technologies, Inc., Kanagawa, Japan). A metal mask defined the cell active area to be 0.16 cm^2. To analyze the electron behaviors in QDSCs, electrochemical impedance spectra (EIS) were measured using an impedance analyzer (PGSTAT 302N, Autolab, Eco-Chemie, The Netherlands) at open-circuit potentials under 1 sun of illumination, with the magnitude and frequency of the alternative signal being 10 mV and 10^{-1}−10^5 Hz, respectively. Impedance spectra were analyzed using an equivalent circuit model, and the model parameters were obtained by Nova software.

3. RESULTS AND DISCUSSION

The synthetic procedure was developed by following the modified protocol (ligand-controlled thermal decomposition)[37] for the preparation of $CuInS_2$ QDs using CuI and $In(Ac)_3$ as copper and indium sources, respectively, as well as 1-dodecanethiol as the reactant for the sulfur source, capping ligands, and solvent. During heat treatment, monomers accumulated in the 1-dodecanethiol solution, and burst nucleation occurred, generating seeds with a concentration above the critical value. With an increase in temperature, the color of the reaction solution gradually changed from colorless to green, yellow, and finally red, suggesting nucleation and subsequent growth of $CuInS_2$ QDs. Figure 1 shows the

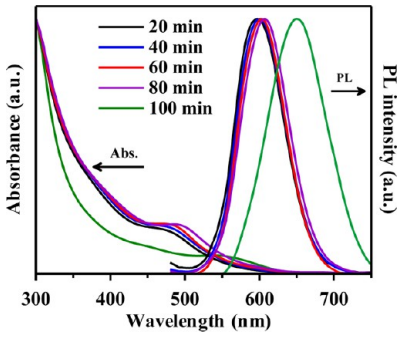

Figure 1. Temporal evolution of normalized absorption and PL spectra of $CuInS_2$ QDs grown at 200 °C.

absorption and emission spectra of $CuInS_2$ QDs versus time. The growth occurred gradually over 100 min of reaction time, as indicated by the increasing red shift in Figure 1. In addition, the appearance of the first exciton peak in the absorption spectrum indicates a relatively narrow size distribution or minimization of nonradiative recombination at surface sites of the as-prepared $CuInS_2$ QDs.

As shown in Figure 2a, the $CuInS_2$ QDs were quasispherical particles with an average diameter of about 2.5 ± 0.5 nm. The existence of well-resolved lattice planes in the inset of Figure 2a

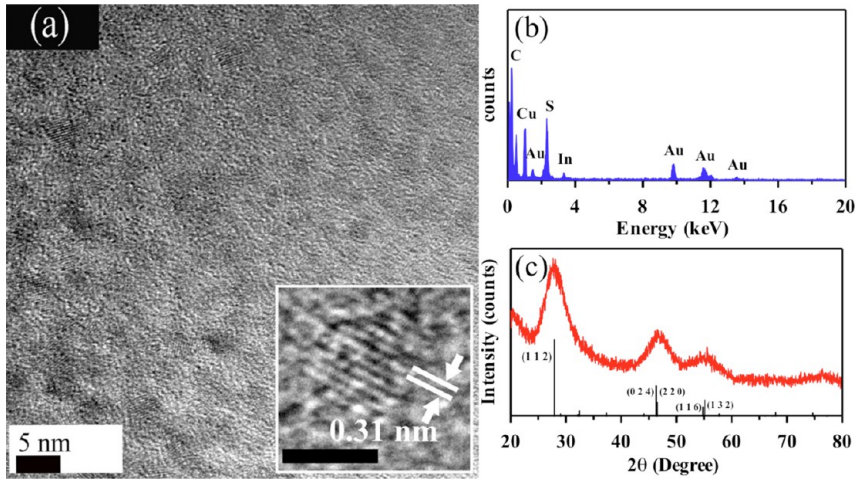

Figure 2. (a) TEM image of the as-prepared $CuInS_2$ QDs. The inset shows that the QDs are crystalline with a lattice fringe of 0.31 nm. The scale bar is 2 nm in the inset of panel a. (b) EDS spectrum and (c) powder XRD patterns of $CuInS_2$ QDs. Au signals are due to the carbon-coated gold grid used in the measurements. The XRD patterns of $CuInS_2$ (JCPDS 47-1372) are also shown as a reference.

demonstrates the good crystallinity of the QDs; moreover, the lattice spacing between two adjacent planes was ~0.31 nm, which corresponds to the (112) lattice planes of chalcopyrite $CuInS_2$ (JCPDS 47-1372). EDS measurement results shown in Figure 2b indicate that the QDs were composed of copper, indium, and sulfur elements. The XRD patterns of the $CuInS_2$ QDs shown in Figure 2c consist of three major peaks at 2θ values of 27.7°, 46.6°, and 55.2°, corresponding to the (112), (220), and (312) indices, respectively, of the tetragonal $CuInS_2$ crystal structure (JCPDS card 47-1372). These peaks are relatively broad, indicating small crystalline particles in the as-prepared $CuInS_2$ QDs.

To evaluate the photovoltaic performance of a QDSC fabricated by employing the as-prepared $CuInS_2$ QDs, it was necessary for these QDs, initially synthesized in an organic solvent, to be transformed into an aqueous phase when the QDs were immobilized on the hydrophilic surface of a TiO_2 electrode film in the aqueous phase. As discussed above, 1-dodecanethiol ligands, with strong thiolate anchoring groups connected to the surface atoms of $CuInS_2$, are often good choices for synthesizing the QDs.[35−42] Therefore, each $CuInS_2$ QD was coated with a densely packed monolayer of 1-dodecanethiol capping ligand; the strong binding of the ligand also prevented its desorption from the QD surface. The direct approach of ligand exchange involving the use of MPA as the ligand resulted in the aggregation of QDs when they were transferred to aqueous media. This could be the result of undesired ligand exchange or insufficient replacement because both MPA and 1-dodecanethiol possess an identical thiolate group for coordination with the surface of $CuInS_2$ QDs. To achieve a more efficient ligand exchange, anchoring of the MPA ligands to the QDs could be circumvented via an indirect approach involving initial weakening of the native ligand of a QD and subsequent displacement of the native ligand. In a previous work,[45] we have shown the effective use of alkyl capping ligands for realizing phase transfer of $AgInS_2$/ZnS QDs. Moreover, after this transfer, the QDs remarkably retained their optical properties. On the basis of the above-mentioned results, the as-prepared $CuInS_2$ QDs in the current study were encapsulated by OA ligands, and this allowed for facile phase transfer of the QDs to aqueous solvents.

Scheme 1 illustrates our ligand-exchange scheme for the QDs, which was affected using a two-step method. In the first step, a $CuInS_2$ QD solution was homogeneously mixed with OA ligands in a mixture of hexane and water with the assistance of ultrasonication. As a result, the aliphatic side of OA ligands spontaneously formed an interdigitated bilayer with the capping agents on the surface of the QDs through hydrophobic van der Waals interactions and a carboxylic region of OA ligands exposed on the outermost surface of the QDs.[45,46] QDs with this nanoarchitecture are referred to as OA($CuInS_2$) QDs. The carboxylic region of the OA ligands on the surface of the OA($CuInS_2$) QDs facilitated the phase transfer from the oil to the water phase. In the second step, the resultant OA($CuInS_2$) QDs were mixed with the bifunctional molecular linker, MPA, in an aqueous phase for 1 h, resulting in ligand exchange. The obtained QDs are abbreviated as MPA($CuInS_2$) QDs. These processes were primarily driven by the law of mass action. Such fast reaction kinetics is primarily the result of the lower

Scheme 1. Schematic Illustration of a Two-Step Ligand Exchange Process[a]

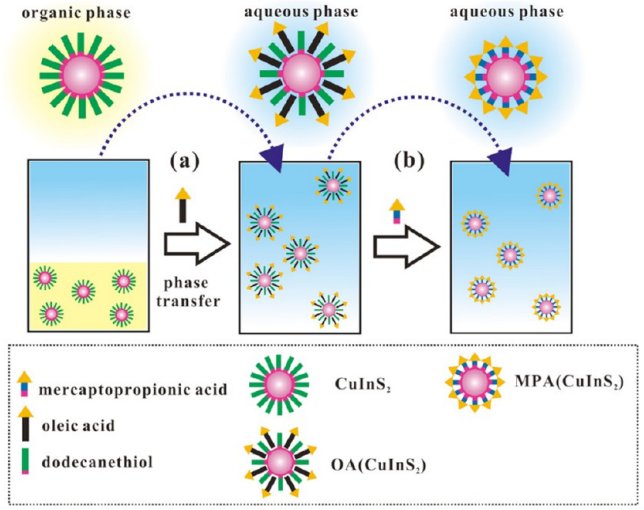

[a](a) Foreign-ligand insertion and (b) alternative-ligand replacement.

diffusion barrier for the hydrophilic MPA ligand in the neat aqueous phase. In other words, the hydrophilic MPA ligand in the aqueous phase possessed higher mobility and transport rate, thereby resulting in a higher probability for the exchange of $CuInS_2$ QDs than the probability for conventional ligand exchange, which is generally performed using a mixture of organic and aqueous phases. Moreover, at this stage, the OA and 1-dodecanethiol ligands in the interdigitated bilayer, formed on the surface of $CuInS_2$ QDs, were more easily and effectively accessible for displacement by MPA than in the case of pristine $CuInS_2$ QDs with only 1-dodecanethiol as the surface ligand. This is because the native surface ligand (1-dodecanethiol) on $CuInS_2$ QDs loosened their dense organization by inserting a foreign ligand (OA). This also facilitated the replacement of the original surface ligands by MPA.

To assess the colloidal stability of $CuInS_2$ QDs, the as-prepared MPA($CuInS_2$) QDs and other water-soluble QDs generated by conventional ligand exchange were dissolved in an aqueous phase under the same conditions. The corresponding water-soluble QDs that underwent ligand exchange via the conventional one-pot method are denoted as CIS@MPA QDs. The photographs in Figure S1 (Supporting Information) clearly show the large difference in the solubility of water-soluble $CuInS_2$ QDs. A visual inspection of the MPA($CuInS_2$) QD solutions modified by our approach showed no indication of flocculation or aggregation after 1 month. In contrast, a solution of CIS@MPA QDs began to precipitate within 1 day and yielded black nanocrystals after 1 month. These results can be possibly attributed to (i) the displacement of native surface ligands from QD surfaces by the MPA ligand, leading to the occurrence of abundant surface defects, and (ii) QDs being expected to exhibit susceptibility to chemical oxidation (especially under photolysis) because of insufficient protection.[47] The absorbance and emission spectra of the pristine QDs dissolved in hexane and of the resulting QDs after ligand exchange dissolved in water are shown in Figure 3a. The intensities of the absorption and emission peaks were normalized. The wavelength of the maximum photoluminescence (PL) emission position (PL λ_{max}) for the pristine $CuInS_2$ QDs is around 602 nm. Compared with the spectra of pristine QDs, the peak shape of the spectra of OA($CuInS_2$) and MPA($CuInS_2$) QDs did not change, but a red shift (10 nm) in the PL peak position and a small change in the full-width at half-maximum values of the emission peak were observed. Still, an excitonic peak in Figure 3a was observed for all QDs. These results suggest that our approach as well as conventional ligand exchange was successfully affected upon phase transfer. Figure 3b shows the photographs of pristine $CuInS_2$ QD samples coated with the original ligand (1-dodecanethiol) in hexane and MPA($CuInS_2$) QDs in water under ambient light (left panel) and UV irradiation (right panel).

The procedure for the fabrication of the QDSC is described schematically in Scheme 2. TiO_2 electrodes were prepared by screen printing of a TiO_2 slurry on an FTO substrate. The SEM image (Figure 4) shows a TiO_2 electrode that contained a porous nanocrystalline film at the bottom to act as a sensitizer absorption layer as well as a larger nanocrystalline film on top for light scattering. Subsequently, the ligand-mediated self-assembly, in which the mesoporous TiO_2 film was pretreated by a bifunctional molecular linker, MPA, was adapted to tightly tether the ex situ synthesized $CuInS_2$ QDs to the TiO_2 surface (denoted as MPA($CuInS_2$)-based QDSC hereafter). It has been

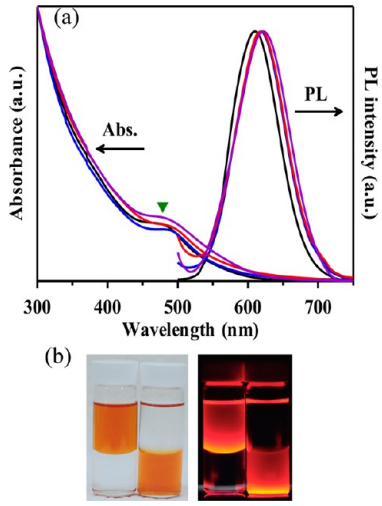

Figure 3. (a) Normalized absorption and PL spectra (λ_{ex} = 430 nm) of as-prepared $CuInS_2$ QDs (black lines) in chloroform and OA($CuInS_2$) (blue lines), MPA($CuInS_2$) (red lines), and CIS@MPA (purple lines) QDs in aqueous media. The green triangle indicates an excitonic absorption peak. (b) Photographs showing $CuInS_2$ QDs in chloroform (bottom layer) before and in water (top layer) after being encapsulated by MPA capping ligands under irradiation with 365 nm ultraviolet light from a UV lamp (right); the left image shows the corresponding samples observed under ambient light.

Scheme 2. Schematic of $CuInS_2$-Based QDSC Fabrication[a]

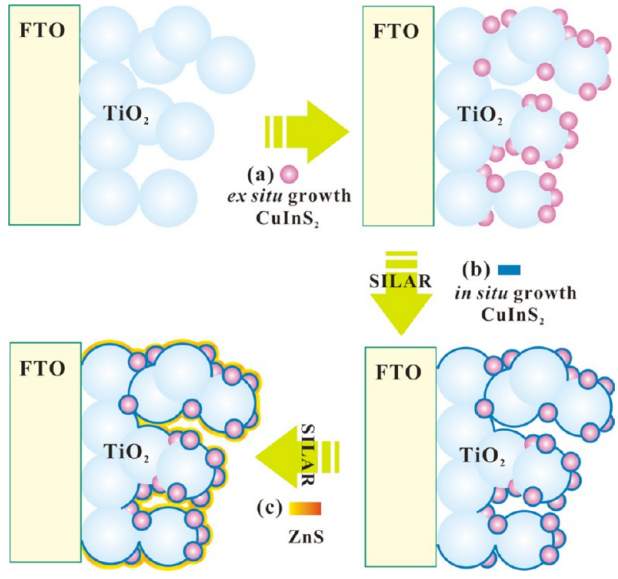

[a](a) Deposition of ex situ pre-existing $CuInS_2$ QDs followed by the use of SILAR process for depositing (b) an in situ generated $CuInS_2$ sensitized layer and (c) a ZnS passivation layer.

reported that MPA molecular linkers coordinated to surface Ti^{4+} sites of TiO_2 through the terminal carboxyl group act as deprotonated carboxylates, whereas thiolate end groups of MPA molecular linkers act as chelating agents on the surface of $CuInS_2$ QDs.[48] Then, using the SILAR process, in which substrates were immersed sequentially into anion and cation precursor solutions, an additional thin layer of $CuInS_2$ was homogeneously and uniformly coated on the surface of the pre-existing $CuInS_2$ QDs, preventing the blockage of nanochannels. A sample obtained after m SILAR cycles of $CuInS_2$ deposition

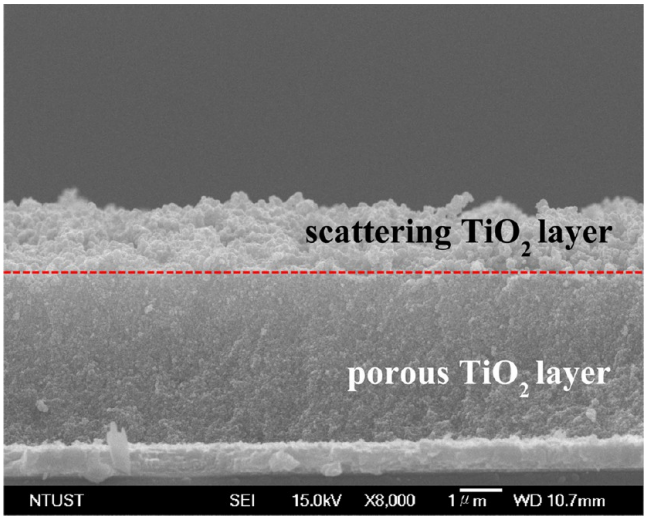

Figure 4. SEM cross section of a TiO_2 electrode composed of porous TiO_2 and scattering TiO_2 layers.

on the $CuInS_2$(m)-based QDSC is denoted as MPA($CuInS_2$)/$CuInS_2$(*m*)-based QDSC. For obtaining a passivation layer, a wide band gap ZnS (3.7 eV in bulk) layer was immobilized onto the as-prepared photoanode by the same SILAR process to prevent the leakage of current from QDs to the electrolyte. For fabricating the QDSC, the resulting photoanode was sandwiched together with a Cu_2S-coated cathode, and a polysulfide electrolyte was employed as a hole scavenger.

Figure 5a,b show the photovoltaic performance of the $CuInS_2$-based QDSCs under the illumination of a solar simulator at one sun (AM 1.5G, 100 mW cm^{-2}); the main photovoltaic parameters are listed in Table 1. It can be seen that the short-circuit current density (J_{SC}), open-circuit voltage (V_{OC}), and fill factor (FF) of sample S1 are 1.36 mA cm^{-2}, 535 mV, and 50.8%, respectively. When OA($CuInS_2$) QDs underwent ligand exchange with MPA, the J_{SC} and V_{OC} of sample S2 increased to 2.30 mA cm^{-2} and 545 mV, respectively, yielding a PCE of 0.64%, which is better than those obtained in previous studies.[24,49] Moreover, the data suggest that the photocurrent originating from the configuration of sample S2 (J_{SC} = 2.30 mA cm^{-2}) was nearly three times the photocurrent originating from the configuration of sample S3 (J_{SC} = 0.71 mA cm^{-2}), which showed the lowest efficiency of 0.18%. As will be discussed later, this dramatic decrease in the J_{SC} for sample S3 was attributed to poor ligand exchange that resulted in an increasing of the extent of surface trapping on the surface of QDs and a disabling of electron transport and charge collection.

To improve the photovoltaic performance, the SILAR process was subsequently employed to allow more $CuInS_2$ to deposit on ex situ synthesized $CuInS_2$ QDs; the *J*–*V* characteristics of such a cell are shown in Figure 5b. Compared with the values for sample S2, further deposition of $CuInS_2$ by the SILAR process caused an increase in the J_{SC} and V_{OC} of sample S4, from 2.30 to 3.78 mA cm^{-2} and from 545 to 565 mV, respectively, thus yielding a ~58% increase in overall efficiency. When the number of SILAR cycles was increased to five, the best photovoltaic performance was obtained: J_{SC} = 7.72 mA cm^{-2}, V_{OC} = 570 mV, FF = 41.8%, and PCE = 1.84%, yielding a ~190% increase in the overall efficiency over that for sample S2. The increase in J_{SC} can be attributed to the increased amount of $CuInS_2$ loading by the SILAR process that

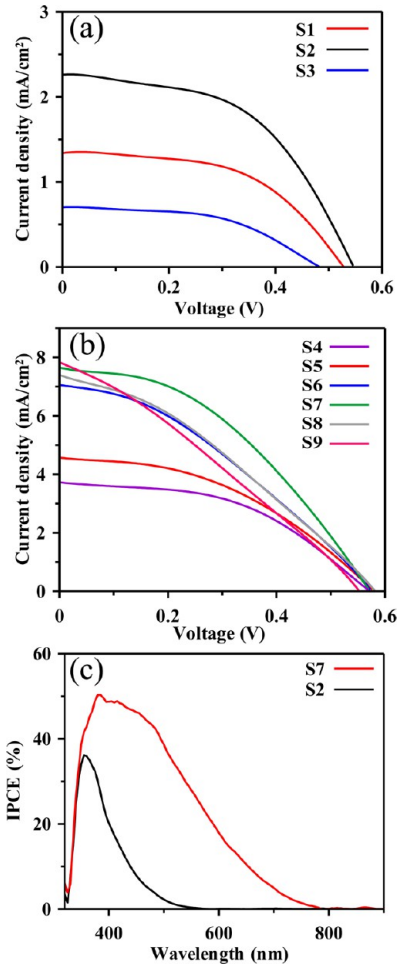

Figure 5. (a, b) *J*–*V* characteristic curves and (c) IPCE of $CuInS_2$-based QDSC fabricated under different sensitization conditions in the presence of a ZnS passivation layer and measured at a light intensity of 100 mW cm^{-2} (AM 1.5G).

Table 1. Photovoltaic Parameters for $CuInS_2$-Based QDSCs Fabricated under Different Sensitization Conditions in the Presence of a ZnS Passivation Layer

sample	condition	J_{SC} (mA cm^{-2})	V_{OC} (mV)	FF (%)	PCE (%)
S1	OA($CuInS_2$)	1.36	535	50.8	0.37
S2	MPA($CuInS_2$)	2.30	545	50.6	0.64
S3	CIS@MPA	0.71	475	52.1	0.18
S4	MPA($CuInS_2$)/$CuInS_2$(2)	3.78	565	47.3	1.01
S5	MPA($CuInS_2$)/$CuInS_2$(3)	4.63	575	42.0	1.12
S6	MPA($CuInS_2$)/$CuInS_2$(4)	7.08	575	34.6	1.41
S7	MPA($CuInS_2$)/$CuInS_2$(5)	7.72	570	41.8	1.84
S8	MPA($CuInS_2$)/$CuInS_2$(6)	7.38	580	33.1	1.42
S9	$CuInS_2$(5)	7.87	555	29.1	1.27

resulted in an increase in light harvesting and in the number of electrons being injected into the TiO_2 film. When compared to "pure" $CuInS_2$-based QDSCs without the presence of cadmium or lead chalcogenide, the PCE (1.84%) of our configuration is better than those obtained in previous studies. For example, Li et al. demonstrated that the devices based on $CuInS_2$ QDs have

dx.doi.org/10.1021/am403531q | ACS Appl. Mater. Interfaces 2013, 5, 11296–11306

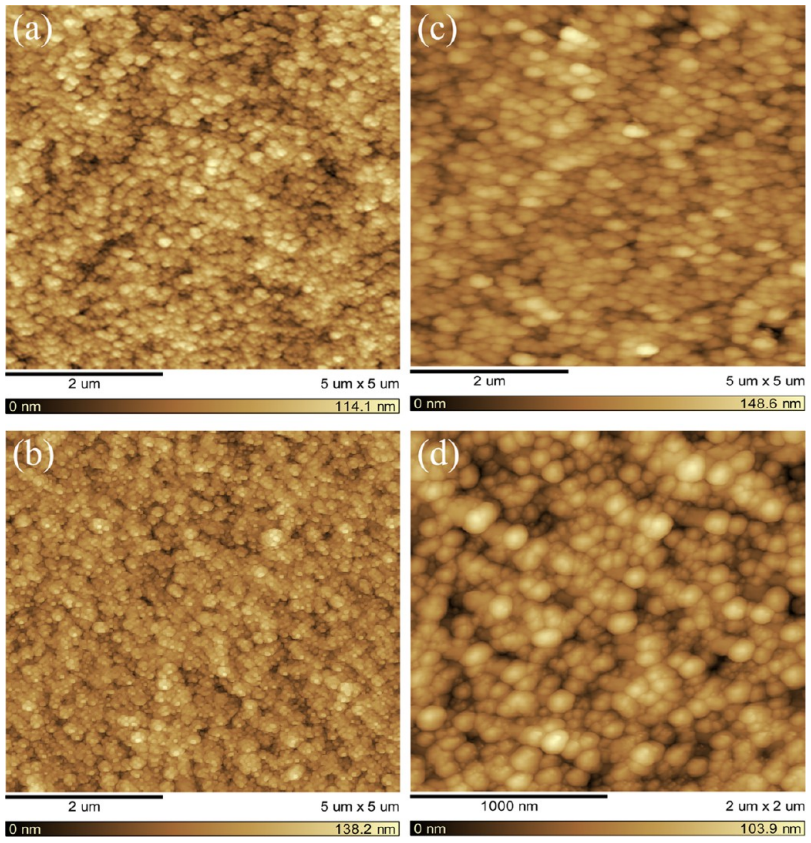

Figure 6. Tapping-mode AFM images of different photoelectrodes: (a) bare TiO_2 porous film, (b) sample S2, and (c) sample S7. The dimensions of the scanned area are 5 × 5 μm^2. (d) High-magnification image of sample S2 (2 × 2 μm^2).

a low PCE of 0.31%.[24] A recent method developed by Hu and co-workers employed aqueous colloidal $CuInS_2$ in QDSCs resulted in a PCE of 0.38%.[23] Santra et al. reported the electrophoretic deposition of $CuInS_2$ colloids within the mesoscopic TiO_2 film offers a PCE of 1.14%.[27] The IPCE spectra for the corresponding cells are shown in Figure 5c. The spectra clearly reveal that the IPCE of sample S7 was significantly higher than that of sample S2 across the visible spectrum, which was in good agreement with the corresponding high J_{SC} value of sample S7. In a control experiment, the PCE decreased dramatically when the ex situ synthesized $CuInS_2$ QDs were not pretreated: from 1.84% for sample S7 to 1.27% for sample S9. This result indicates that the ex situ synthesized $CuInS_2$ QDs play an important role in improving the photovoltaic performance. According to the basic principle of the classical nucleation theory, the activation energy for heterogeneous nucleation is much lower than that for homogeneous nucleation, thereby preventing independent nucleation. The presence of pre-existing seeds of ex situ synthesized $CuInS_2$ QDs on TiO_2 electrodes could considerably reduce the activation energy required for in situ $CuInS_2$ nucleation by the SILAR process. Therefore, $CuInS_2$ preferentially starts growing on the existing ex situ synthesized $CuInS_2$ QDs by the SILAR process in solution. Similar performance enhancement in a photovoltaic device has been reported previously by using ex situ synthesized CdS QDs acting as a seed layer on mesoporous TiO_2 to induce the nucleation and growth of CdSe QDs in a QDSC. In this case, the efficiency achieved by the cell with a seed layer (2.1%) was significantly higher that achieved in the absence of a seed layer (1.4%).[50] Furthermore, Tian et al.[51] also demonstrated that a CdS layer can serve as a seed layer to enhance the CdSe growth rate in a QDSC.

The SEM image (see Supporting Information Figure S2) shows the TiO_2 electrode fabricated by the combined ex situ/in situ growth, which revealed no difference in the cross-section region as compared to Figure 4. AFM imaging in the tapping mode was utilized to determine the overall surface roughness and to obtain topographical images, as shown in Figure 6. Histograms depicting the size distribution for each sample are shown in Figure S3 (Supporting Information). Figure 6a displays the AFM image of a bare TiO_2 porous film, which was screen-printed onto an FTO glass substrate. The film was found to be composed of nearly spherical particles that were closely packed. The rms of the surface was 16.87 nm. The AFM image of sample S2 without a scattering TiO_2 layer in Figure 6b shows a blurred morphology with a rms of 14.29 nm, indicating that the TiO_2 surface was heterogeneously covered by $CuInS_2$ QDs. This is clearly seen in the high-magnification image (Figure 6d) that shows many islandlike shapes distributed on the surface of TiO_2 nanoparticles, suggesting that well-dispersed individual MPA($CuInS_2$) QDs were tethered to TiO_2 nanoparticles. Using the SILAR process, an additional thin layer of $CuInS_2$ was coated on the surface of the pre-existing $CuInS_2$ QDs. In Figure 6c, the rms of sample S7 without a scattering TiO_2 layer is 11.72 nm, revealing a relatively smoother surface than other samples. This may be attributed to layer-by-layer growth of $CuInS_2$ during the SILAR process, resulting in roughness reduction and grain growth.

To study the decay behaviors of $CuInS_2$ QDs dissolved in solution (samples L1−L4) or anchored onto TiO_2 films (samples L5−L7) in more detail, the kinetic curves for the

representative emission of each sample were recorded with 450 nm diode laser excitation, as shown in Figure 7. Details of the spectroscopic and fitting parameters for the emission decays with reduced χ^2 ($\leq$1.1) for each sample are summarized in Table 2.

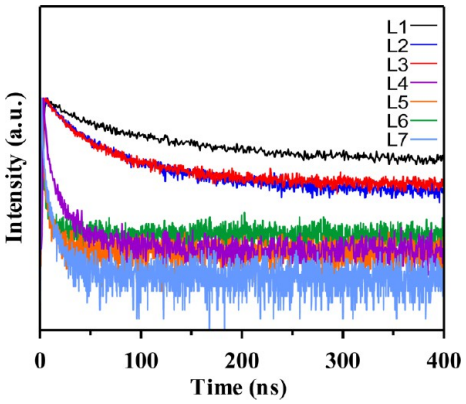

Figure 7. Normalized photoluminescence decay dynamics of different samples recorded at room temperature.

The emission decay data were fit to a biexponential decay function

$$I = A_1 \exp(-t/\tau_1) + A_2 \exp(-t/\tau_2) \quad (2)$$

where I is the normalized emission intensity, A_1 and A_2 are the amplitudes of decay components, t is the time after pulsed-laser excitation, and τ_1 and τ_2 are lifetimes of the decay components. The average excited-state lifetime is calculated as

$$\tau_{ave} = \frac{A_1\tau_1^2 + A_2\tau_2^2}{A_1\tau_1 + A_2\tau_2} \quad (3)$$

The obtained emission decay curves clearly indicate the existence of two decay kinetics processes: slow decay (τ_1) and fast decay (τ_2). Typically, the relatively shorter lifetime can be associated with the involvement of surface defects, including vacancies and dangling bonds, whereas the longer one can be attributed to intraband defect levels (i.e., donor–acceptor pair (DAP) recombination). These observations are similar to those previously reported for I–III–VI QDs.[52−54] The τ_{ave} value for these samples dissolved in solution is in the following ascending order: sample L4 (29.2 ns) < sample L3 (120 ns) < sample L2 (125 ns) < sample L1 (211 ns). Compared with samples L2–L4 in the aqueous phase, sample L1 dissolved in hexane has a slightly larger τ_1 value owing to the intrinsic property of $CuInS_2$. Solutions of samples L2 and L3 showed very similar PL decay characteristics with an average lifetime of ~120 ns. The decrease in the average exciton lifetime for $CuInS_2$ QDs in the aqueous phase is due to an increase in surface defects. Compared to sample L3 prepared by our new approach, sample L4 showed a dramatic lifetime shortening for both components with an average lifetime of 29.2 ns. Amplitude A_2 of the shorter lifetime component accounts for nearly 80% of the total PL decay, which suggests that fast trapping processes are dominant in sample L4. This observation clearly indicates poor surface reconstruction with plenty of recombination centers and the contribution of surface defects created during the one-pot ligand-exchange process. Concurrently, the quantum yield (Φ) of samples L2 and L3 in an aqueous solution were measured to be 0.61 and 0.51%, respectively. These values are lower than that for the pristine sample L1 (Φ = 0.95%) but are higher than that for the water-soluble sample L4 (Φ = 0.18%) prepared by the conventional one-pot synthesis. Typically, Φ is equal to or correlated with the ratio of the radiative decay rate to the sum of the radiative and nonradiative decay rates, which is given by $\Phi = k_R/(k_R + k_{NR}) = k_R \times \tau_{ave}$, where k_R is the radiative decay rate and k_{NR} is the nonradiative decay rate.[55] Table 2 lists the radiative and nonradiative decay rates for samples L1–L4. The nonradiative decay rate constant was calculated to be 7.98 and 8.28 μs^{-1} for samples L2 and L3, respectively. Upon further calculation, the nonradiative decay rate constant for sample L4 was found to be dramatically higher than those for samples L1–L3 at 34.2 μs^{-1} and is associated with the corresponding lowest quantum yield. This result could be ascribed to abundant surface defects in L4, providing nonradiative recombination sites and giving rise to a decline in the PL intensity of the sample.

Under steady-state illumination, the photoexcited $CuInS_2$ QDs exhibited electron (e^-)–hole (h^+) separation followed by charge carrier recombination via radiative or nonradiative processes (i.e., eq 4). When in contact with TiO_2, the photoexcited $CuInS_2$ QDs were capable of injecting electrons into the conduction band of TiO_2 (i.e., eq 5). The photoinduced reactions between $CuInS_2$ and TiO_2 are summarized in eqs 4–6.

$$CuInS_2 + h\upsilon \rightarrow CuInS_2(e^- + h^+) \quad (4)$$

$$CuInS_2(e^- + h^+) \rightarrow CuInS_2 + h\upsilon' \quad (5)$$

$$CuInS_2(e^-) + TiO_2 \rightarrow CuInS_2 + TiO_2(e^-) \quad (6)$$

Therefore, after the attachment of QDs on the TiO_2 surface, a decrease in lifetime is expected because of the participation of excited $CuInS_2$ QDs in injecting electrons into TiO_2, as shown in Table 2. Sample L6 showed the lowest average lifetime of 9.5 ns, indicating that photoexcited $CuInS_2$ QDs formed by in situ and ex situ QD growth benefit from the transfer of electrons

Table 2. Fluorescence Lifetime Parameters for Different Samples

sample	condition	A_1 (%)	τ_1 (ns)	A_2 (%)	τ_2 (ns)	τ_{ave} (ns)	Φ (%)	k_R (μs^{-1})	k_{NR} (μs^{-1})	k_{ET} (μs^{-1})	χ^2
L1	$CuInS_2$[a]	55.9	283	44.1	50.8	211	0.95	0.05	4.69		1.00
L2	OLA($CuInS_2$)[b]	43.0	154	57.1	40.2	125	0.61	0.05	7.98		1.03
L3	MPA($CuInS^2$)[b]	39.0	151	61.0	34.6	120	0.51	0.04	8.28		1.04
L4	CIS@MPA[b]	20.2	45.5	79.8	9.48	29.2	0.18	0.06	34.2		0.96
L5	MPA($CuInS_2$)[c]	22.2	16.4	77.8	2.55	11.5				78.6	1.01
L6	MPA($CuInS_2$)/$CuInS_2$(5)[c]	28.1	8.78	71.9	1.08	6.94				136	1.07
L7	CIS@MPA[c]	20.0	20.6	80.0	3.47	13.7				38.6	1.00

[a]Sample dissolved in hexane. [b]Sample dissolved in water. [c]Sample deposited on TiO_2 surface

into the conduction band of TiO_2 that concurrently contributes to the enhancement in J_{SC}, as listed in Table 1.

The charge-transfer rate constant (k_{ET}) can be estimated by comparing the lifetimes of $CuInS_2$ QDs dissolved in the solution and anchored on TiO_2 surface by using the following equation:

$$k_{ET} = \frac{1}{\tau_{(CuInS_2/TiO_2)}} - \frac{1}{\tau_{(CuInS_2)}} \quad (7)$$

The transfer rate constants for injection from QDs to metal oxides have previously been reported with values of 10^7-10^{11} s^{-1}.[27,32,56−60] For example, it was previously reported that for electron transfer from CdSe to TiO_2 via MPA the transfer rate constant values range from 1.0×10^7 to 2×10^{11} s^{-1}.[57−59] Makhal et al. reported that the transfer rate constant for electron transfer is 2.9×10^8 s^{-1} from 4.2 nm CdSe to TiO_2.[60] The transfer rate constant for Zn-$CuInS_2$/ZnO[32] and $CuInS_2$/TiO_2[27] were found to be 2.39×10^8 and 5.75×10^{11} s^{-1}, respectively. In our case, k_{ET} values obtained from emission quenching were 7.86×10^7 and 1.36×10^8 s^{-1} for samples L5 and L6, respectively. The higher transfer rate constant for sample L6 indicates significantly more electron injection from $CuInS_2$ to TiO_2. This result is consistent with the corresponding high current density of 7.72 mA cm^{-2} for sample S7, which was nearly three times that for sample S2 that lacked in situ QD growth. For comparison, CIS@MPA QDs were deposited on the TiO_2 surface, and the k_{ET} value obtained by comparing the lifetimes of samples L4 and L7 was 3.86×10^7 s^{-1}. The rate constant for electron transfer for sample L7 was deduced to be similar in magnitude that that for samples L5 and L6. However, a significantly low photovoltaic performance for sample S3 QDSC is observed in Table 1. This observation clearly suggests that the number of electrons trapped at nonradiative defect sites of CIS@MPA is greater than the number of electrons injected from photoexcited QDs to the conduction band of TiO_2 because of insufficient ligand replacement, which was performed according to the conventional protocol.

To gain further insight into the electron transport and recombination properties of QDSCs, we utilized EIS at open-circuit voltage under one sun illumination to investigate the resistance of electron transfer in QDSCs for samples S2, S7, and S9. Figure 8a shows the Nyquist curves containing two semicircles in the high-frequency (>1 kHz) and low-frequency regions (10−100 Hz). These curves represent the interfacial charge-transfer resistances of the cells. Each semicircle in the Nyquist curves can be modeled with electrical elements (e.g., resistance, R_{ct}) and constant phase element (CPE) to describe the interfacial properties, internal resistance, and charge-transfer kinetics. By fitting the experimental data with an equivalent circuit simulation (Figure 8b) containing a series resistance (R_s), resistances at the counter electrode/electrolyte interface (R_{ct1}) and at the TiO_2/QDs/electrolyte interface (R_{ct2}) could be obtained (Table 3).

We observed that the R_s values for all cells were similar because of the utilization of identical counter electrodes (Cu_2S/FTO glass). The lower R_{ct1} values for all the electrodes imply a lower electron-transfer resistance at the counter electrode/electrolyte interface. Sample S7 showed the lowest R_{ct2} value of 171 Ω, which is lower than the values for both sample S2 (627 Ω) and sample S9 (297 Ω). We hypothesize that these results are due to to the combined synergetic effects of in situ and ex

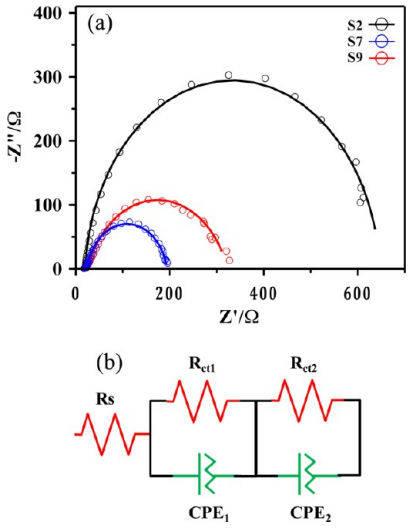

Figure 8. (a) Nyquist plots obtained from impedance spectra of QDSCs fabricated under different sensitization conditions. (b) Corresponding equivalent circuit model simulated to fit the impedance spectra. The symbols and solid lines represent experimental and fitted results, respectively, according to the equivalent circuit model.

Table 3. EIS Parameters Determined by Fitting the Impedance Spectra of QDSCs Fabricated under Different Sensitization Conditions

sample	R_s (Ω)	R_{ct1} (Ω)	R_{ct2} (Ω)
S2	17.0	2.82	627
S7	18.6	5.12	171
S9	18.8	7.20	297

situ $CuInS_2$ QD growth, which facilitated more electron injection from the QD sensitizers into TiO_2. Because of the high surface-to-volume ratio of QDs, their surface properties should significantly affect their structural, optical, and electrical properties. In particular, because defects (such as unpassivated surface atoms) at QD surface sites act as temporary "surface traps" for a carrier, the presence of surface defects hinders charge transfer into the TiO_2 conduction band and therefore greatly reduces the PCE of a QDSC. As mentioned previously, the SILAR process provides nucleation and an in situ growth mechanism that result in high surface coverage on pre-existing $CuInS_2$ QDs, leading to a significant reduction in surface-related defect states and a certain improvement in the quantum yield of the QDs. As a result, better photovoltaic performance was achieved for the sample S7 QDSC. This result agrees well with the results of the IPCE and $J-V$ curves.

4. CONCLUSIONS

$CuInS_2$ QDSCs with high photovoltaic performance were fabricated via an eco-friendly approach by using less hazardous precursors than are currently used. Our method utilizes the advantages of the ex situ synthesis approach with highly crystalline $CuInS_2$ QDs and the in situ SILAR approach with a high surface coverage of $CuInS_2$ QDs. A water-soluble phase of the ex situ synthesized $CuInS_2$ QDs is readily obtained through a two-step ligand-exchange process under the assistance of ultrasonication. This is an efficient pathway that can be carried out with low energy consumption (ambient temperature) and a short reaction time (less than 2 h). In contrast to the conventional one-pot protocol for preparing water-soluble

QDs, our method preserves the higher PL intensity of QDs as well as their long-term stability for more than 1 month. The decay kinetic curves for $CuInS_2$ QDs dissolved in solution or anchored to TiO_2 films were recorded with 450 nm diode laser excitation. A decay lifetime of 120 ns was measured for MPA($CuInS_2$) QDs prepared in an aqueous solution, whereas it was only 9.5 ns for MPA($CuInS_2$)/$CuInS_2$(5)/TiO_2, indicating its k_{ET} value to be 1.36×10^8 s^{-1}. Results obtained using $J-V$ curves indicate that the J_{SC}, V_{OC}, and FF of the MPA($CuInS_2$)-based QDSC are 2.30 mA cm^{-2}, 545 mV, and 50.6%, respectively, which lead to a PCE of 0.64%. After the in situ growth of QDs by the SILAR process on the TiO_2 surface with the pre-existing seeds of ex situ synthesized $CuInS_2$ QDs, the MPA($CuInS_2$)/$CuInS_2$(5)-based QDSC showed a PCE of 1.84%; this value was higher by approximately 180 and 45% than the PCEs shown by $CuInS_2$ QDSCs formed by ex situ and in situ growth, respectively. The IPCE of MPA($CuInS_2$)/$CuInS_2$(5)-based QDSC was significantly higher than that of MPA($CuInS_2$)-based QDSCs across the visible spectrum, which was in good agreement with the corresponding high J_{SC} value of MPA($CuInS_2$)/$CuInS_2$(5)-based QDSC. According to EIS results, the cell derived from the MPA($CuInS_2$)/$CuInS_2$(5) configuration had the lowest R_{ct2} of 171 Ω, suggesting that the combined synergetic effects of in situ and ex situ $CuInS_2$ QD growth facilitate more electron injection from the QD sensitizers into TiO_2. Thus, the results show that the proposed procedure is eco-friendly and commercially viable and that it will show significant promise in the future. Furthermore, it can be extended to other cadmium-free QD sensitizers such as I–III–VI_2 (I = Cu and Ag; III = Al, In, and Ga; VI = S and Se) and I_2–II–IV–VI_4 (I = Cu and Ag; II = Zn; IV = Si, Ge, and Sn; VI = S and Se) materials.

■ ASSOCIATED CONTENT

Supporting Information

Photographs of the colloidal stability of aqueous QDs for various amounts of time; SEM images of a TiO_2 electrode fabricated by the combined ex situ/in situ growth; and size distribution histograms for the TiO_2 photoanode as obtained from AFM images. This material is available free of charge via the Internet at http://pubs.acs.org.

■ AUTHOR INFORMATION

Corresponding Author

*E-mail: jychang@mail.ntust.edu.tw. Tel.: +886-2-27303636. Fax: +886-2-27376644.

Notes

The authors declare no competing financial interest.

■ ACKNOWLEDGMENTS

We thank the National Science Council of the Republic of China for financially supporting this research under contract no. NSC 102-2628-M-011-001-MY3.

■ REFERENCES

(1) Grätzel, M. *Acc. Chem. Res.* **2009**, *42*, 1788–1798.
(2) Yella, A.; Lee, H.-W.; Tsao, H. N.; Yi, C.; Chandiran, A. K.; Nazeeruddin, M.; Diau, E. W.-G.; Yeh, C.-Y.; Zakeeruddin, S. M.; Grätzel, M. *Science* **2011**, *334*, 629–634.
(3) Snatra, P. K.; Kamat, P. V. *J. Am. Chem. Soc.* **2012**, *134*, 2508–2511.
(4) Beard, M. C.; Midgett, A. G.; Hanna, M. G.; Luther, J. M.; Hughes, B. K.; Nozik, A. J. *Nano Lett.* **2010**, *10*, 3019–3027.
(5) Pijpers, J. J. H.; Ulbricht, R.; Tielrooij, K. J.; Osherov, A.; Golan, Y.; Delerue, C.; Allan, G.; Bonn, M. *Nat. Phys.* **2009**, *5*, 811–814.
(6) McGuire, J. A.; Sykora, M.; Joo, J.; Pietryga, J. M.; Klimov, V. I. *Nano Lett.* **2010**, *10*, 2049–2057.
(7) Schaller, R. D.; Agranovich, V. M.; Klimov, V. I. *Nat. Phys.* **2005**, *1*, 189–194.
(8) McGuire, J. A.; Joo, J.; Pietryga, J. M.; Schaller, R. D.; Klimov, V. I. *Acc. Chem. Res.* **2008**, *41*, 1810–1819.
(9) Shockley, W.; Queisser, H. J. *J. Appl. Phys.* **1961**, *32*, 510–519.
(10) Pan, Z.; Zhang, H.; Cheng, K.; Hou, Y.; Hua, J.; Zhong, X. *ACS Nano* **2012**, *6*, 3982.
(11) Zhang, Q.; Guo, X.; Huang, X.; Huang, S.; Li, D.; Luo, Y.; Shen, Q.; Toyoda, T.; Meng, Q. *Phys. Chem. Chem. Phys.* **2011**, *13*, 4659–4667.
(12) Fan, S.-Q.; Fang, B.; Kim, J. H.; Jeong, B.; Kim, C.; Yu, J.-S.; Ko, J. *Langmuir* **2010**, *26*, 13644–13649.
(13) Lan, G.-Y.; Yang, Z.; Lin, Y.-W.; Lin, Z.-H.; Liao, H.-Y.; Chang, H.-T. *J. Mater. Chem.* **2009**, *19*, 2349–2355.
(14) Yang, Z.; Chang, H.-T. *Sol. Energy Mater. Sol. Cells* **2010**, *94*, 2046–2051.
(15) Ning, Z.; Tian, H.; Yuan, C.; Fu, Y.; Qin, H.; Sun, L.; Ågren, H. *Chem. Commun.* **2011**, *47*, 1536–1538.
(16) Chang, J. A.; Rhee, J. H.; Im, S. H.; Lee, Y. H.; Kim, H. -J.; Seok, S. I.; Nazeeruddin, M. K.; Grätzel, M. *Nano Lett.* **2010**, *10*, 2609–2612.
(17) Yu, P.; Zhu, K.; Norman, A. G.; Ferrere, S.; Frank, A. J.; Nozik, A. J. *J. Phys. Chem. B* **2006**, *110*, 25451–25454.
(18) Derfus, A. M.; Chan, W. C. W.; Bhatia, S. N. *Nano Lett.* **2004**, *4*, 11–18.
(19) Kirchner, C.; Liedl, T.; Kudera, S.; Pellegrino, T.; Javier, A. M.; Gaub, H. E.; Stöllzle, S.; Fertig, N.; Parak, W. J. *Nano Lett.* **2005**, *5*, 331–338.
(20) Sato, K.; Yokosuka, S.; Takigami, Y.; Hirakuri, K.; Fujioka, K.; Manome, Y.; Sukegawa, H.; Iwai, H.; Fukata, N. *J. Am. Chem. Soc.* **2011**, *133*, 18626–18633.
(21) Tsoi, K. M.; Dai, Q.; Alman, B. A.; Chan, W. C. W. *Acc. Chem. Res.* **2013**, *46*, 662–671.
(22) Look, D. C.; Manthuruthil, J. C. *J. Phys. Chem. Solids* **1976**, *37*, 173–180.
(23) Hu, X.; Zhang, Q.; Huang, X.; Li, D.; Luo, Y.; Meng, Q. *J. Mater. Chem.* **2011**, *21*, 15903–15905.
(24) Li, T.-L.; Lee, Y.-L.; Teng, H. *Energy Environ. Sci.* **2012**, *5*, 5315–5324.
(25) Chen, C.; Ali, G.; Yoo, S. H.; Kum, J. M.; Cho, S. O. *J. Mater. Chem.* **2011**, *21*, 16430–16435.
(26) McDaniel, H.; Fuke, N.; Pietryga, J. M.; Klimov, V. I. *J. Phys. Chem. Lett.* **2013**, *4*, 355–361.
(27) Santra, P. K.; Nair, P. V.; Thomas, K. G.; Kamat, P. V. *J. Phys. Chem. Lett.* **2013**, *4*, 722–729.
(28) Chang, J.-Y.; Lin, J.-M.; Su, L.-F.; Chang, C.-F. *ACS. Appl. Mater. Interfaces* **2013**, *5*, 8740–8752.
(29) Leschkies, K. S.; Divakar, R.; Basu, J.; Enache-Pommer, E.; Boercker, J. E.; Carter, C. B.; Kortshagen, U. R.; Norris, D. J.; Aydil, E. S. *Nano Lett.* **2007**, *7*, 1793–1798.
(30) Chen, J.; Zhao, D. W.; Song, J. L.; Sun, X. W.; Deng, W. Q.; Liu, X. W.; Lei, W. *Electrochem. Commun.* **2009**, *11*, 2265–2267.
(31) Buhbut, S.; Itzhakov, S.; Tauber, E.; Shalom, M.; Hod, I.; Geiger, T.; Garini, Y.; Oron, D.; Zaban, A. *ACS Nano* **2010**, *4*, 1293–1298.
(32) Kuo, K.-T.; Liu, D.-M.; Chen, S.-Y.; Lin, C.-C. *J. Mater. Chem.* **2009**, *19*, 6780–6788.
(33) Li, T.-L.; Lee, Y.-L.; Teng, H. *Energy Environ. Sci.* **2012**, *5*, 5315–5324.
(34) Basiruddin, S. K.; Saha, A.; Pradhan, N.; Jana, N. R. *J. Phys. Chem. C* **2010**, *114*, 11009–11017.
(35) Li, L.; Daou, T. J.; Texier, I.; Chi, T. T. K.; Liem, N. Q.; Reiss, P. *Chem. Mater.* **2009**, *21*, 2422–2429.
(36) Xie, R.; Rutherford, M.; Peng, X. *J. Am. Chem. Soc.* **2009**, *131*, 5691–5697.

(37) Li, L.; Pandey, A.; Werder, D. J.; Khanal, B. P.; Pietryga, J. M.; Klimov, V. I. *J. Am. Chem. Soc.* **2011**, *133*, 1176−1179.
(38) Park, J.; Kim, S.-W. *J. Mater. Chem.* **2011**, *21*, 3745−3750.
(39) Nam, D.-E.; Song, W.-S.; Yang, H. *J. Mater. Chem.* **2011**, *21*, 18220−18226.
(40) Song, W.-S.; Kim, J.-H.; Lee, J.-H.; Lee, H.-S.; Do, Y. R.; Yang, H. *J. Mater. Chem.* **2012**, *22*, 21901−21908.
(41) Booth, M.; Brown, A. P.; Evans, S. D.; Critchley, K. *Chem. Mater.* **2012**, *24*, 2064−2070.
(42) Xiang, W.-D.; Yang, H.-L.; Liang, X.-J.; Zhong, J.-S.; Wang, J.; Luo, L.; Xie, C.-P. *J. Mater. Chem. C* **2013**, *1*, 2014−2020.
(43) Costi, R.; Saunders, A. E.; Elmalem, E.; Salant, A.; Banin, U. *Nano Lett.* **2008**, *8*, 637−641.
(44) Zhang, W.; Chen, G.; Wang, J.; Ye, B.-C.; Zhong, X. *Inorg. Chem.* **2009**, *48*, 9723−9731.
(45) Fahmi, M. Z.; Chang, J.-Y. *Nanoscale* **2013**, *5*, 1517−1528.
(46) Prakash, A.; Zhu, H.; Jones, C. J.; Benoit, D. N.; Ellsworth, A. Z.; Bryant, E. L.; Colvin, V. L. *ACS Nano* **2009**, *3*, 2139−2146.
(47) Bagaria, H. G.; Kini, G. C.; Wong, M. S. *J. Phys. Chem. C* **2010**, *114*, 19901−19907.
(48) Watson, D. F. *J. Phys. Chem. Lett.* **2010**, *1*, 2299−2309.
(49) Xu, G.; Ji, S.; Miao, C.; Liu, G.; Ye, C. *J. Mater. Chem.* **2012**, *22*, 4890−4896.
(50) Lee, Y.-L.; Haung, B.-M.; Chien, H.-T. *Chem. Mater.* **2008**, *20*, 6903−6905.
(51) Tian, J.; Gao, R.; Zhang, Q.; Zhang, S.; Li, Y.; Lan, J.; Qu, X.; Cao, G. *J. Phys. Chem. C* **2012**, *116*, 18655−18662.
(52) Nose, K.; Omata, T.; Otsuka-Yao-Matsuo, S. *J. Phys. Chem. C* **2009**, *113*, 3455−3460.
(53) Zhong, H.; Zhou, Y.; Ye, M.; He, Y.; Ye, J.; He, C.; Yang, C.; Li, Y. *Chem. Mater.* **2008**, *20*, 6434−6443.
(54) Hong, S. P.; Park, H. K.; Oh, J. H.; Yang, H.; Do, Y. R. *J. Mater. Chem.* **2012**, *22*, 18939−18949.
(55) Jiang, Z.-J.; Leppert, V.; Kelley, D. F. *J. Phys. Chem. C* **2009**, *113*, 19161−19171.
(56) Farrow, B.; Kamat, P. V. *J. Am. Chem. Soc.* **2009**, *131*, 11124−11131.
(57) Robel, I.; Subramanian, V.; Kuno, M.; Kamat, P. V. *J. Am. Chem. Soc.* **2006**, *128*, 2385−2393.
(58) Kongkanand, A.; Tvrdy, K.; Takechi, K.; Kuno, M.; Kamat, P. V. *J. Am. Chem. Soc.* **2008**, *130*, 4007−4015.
(59) Robel, I.; Kuno, M.; Kamat, P. V. *J. Am. Chem. Soc.* **2007**, *129*, 4136−4137.
(60) Makhal, A.; Yan, H.; Lemmens, P.; Pal, S. K. *J. Phys. Chem. C* **2010**, *114*, 627−632.